EUROPEAN JOURNAL OF BIOMEDICAL AND PHARMACEUTICAL SCIENCES
http://www.ejbps.com

ISSN 2349-8870
Volume: 8
Issue: 3
403-412
Year: 2021

THE ROLE OF LIGAND DESIGN AFFECTING THE THERMAL AND LIGHT-INDUCED SPIN TRANSITION IN MONONUCLEAR IRON (II) COMPLEXES

Yackouba Konté[1], Mame Seyni Sylla[1], Aïssatou Sarr[1], Papa Aly Gaye[1], Mamoudou Diallo[1], Cédric Desplanches[2], Philippe Guionneau[2], Guillaume Chastanet[2] and Chérif Baldé[1*]

[1]Laboratoire de Chimie et Physique des Matériaux (LCPM), Université Assane Seck de Ziguinchor, Bp: 523 Ziguinchor, Sénégal.
[2]CNRS, Université de Bordeaux, ICMCB, 87 avenue du Dr. A. Schweitzer, Pessac, 33608, France.

***Corresponding Author: Prof. Chérif Baldé**
Laboratoire de Chimie et Physique des Matériaux (LCPM), Université Assane Seck de Ziguinchor, Bp: 523 Ziguinchor, Sénégal.
DOI: https://doi.org/10.17605/OSF.IO/4XJYB

Article Received on 14/01/2021 **Article Revised on 03/02/2021** **Article Accepted on 24/02/2021**

ABSTRACT
Molecules are increasingly considered for information processing and sensing applications. Therefore, much research has focused on the improvement of such property changes, especially the ability to observe the switching at room temperature. The relationship between chemical structure and spin state in a transition metal complex has an important bearing on the design of spin crossover materials. Thus, ligand design has been the focus of much attention. It has allowed generation of highly cooperative spin-transition iron (II) complexes to promote hysteretic effects. We present herein the thermal and light-induced magnetic properties of several photoswitchable precursors based on a bidentate ligand (phenanthroline), and a monodentate ligand such as a pyridine or picoline derivative. These results were discussed on the basis of the alkyl-substituted pyridine ligand effects on the magnetic and phtomagnetic properties of mononuclear iron (II) complexes. Interestingly, single crystals were obtained for the 4-cyano-pyridine derivate allowing the X-ray diffraction crystal-structure determination.

KEYWORDS: Ligand effect, Iron, Spin crossover, LIESST, Magnetic properties.

1 INTRODUCTION AND BACK GROUND
The recent developments in technology in which molecules or assemblies of molecules are used for information processing has enabled scientists to investigate the potential of molecules in several areas, namely for the development of display and memory devices.[1-10] Among them, the materials that undergo a spin crossover (SCO) phenomena, upon application of external stimuli such as temperature, pressure, light and electric field have received a high interest within the construction of molecular devices with optical switch or/and magneto-optical storage properties.[7-13]

In this context, SCO coordination compounds of $3d^4$ to $3d^7$ electronic configuration displaying a central metallic ion in an octahedral environment have been a focus of research for nearly 90 years.[14] Several aspects of SCO phenomenon have been reviewed in the past.[7-9],[11-13],[15-23] Of these, by far the majority are pseudo-octahedral $3d^6$ iron (II) complexes, thus, as a function of the ligand field strength, the six electron of the iron (II) ion can occupy the 3d orbitals in two different ways giving rise to two different stable states: a diamagnetic low-spin (LS) electronic configuration state $t_{2g}^6e_g^0$ ($^1A_{1g}$, S=0) in case of a strong ligand field and a paramagnetic high-spin (HS) electronic state $t_{2g}^4e_g^2$ ($^5T_{2g}$, S=2) when the ligand field is weak. In the case of an intermediate ligand field, the two spin states may become so close in energy that a small external perturbation can switch between the states.

LS↔HS conversions are accompanied by profound changes in all properties that depend on the distribution of the 3d valence electrons. Besides the most obvious change of magnetic properties, including switchable diamagnetism ↔ paramagnetism,[24] the reversible change of color,[24] refractive index,[25] electrical conductivity,[26] luminescence,[27] nonlinear optical,[28] and mechanical properties[29] may accompany SCO. The spin state change can be induced by various external stimuli such as temperature,[11] pressure,[30] light irradiation,[31,32] magnetic[33] and electric field,[34] guest molecules,[35] and so forth.

Recently, topics such as the role of ligand design in affecting SCO have attracted great interest.[36-40] A Rational ligand design has allowed the generation of a highly cooperative spin-transition iron (II) complex.[36-38]

In this paper, we focus attention on the influence of the alkyl-substituted pyridine ligand on magnetic and photomagnetic properties by determining systematically

the thermal spin transition temperature, $T_{1/2}$, and the relaxation temperature of the photo-induced high-spin state, T(LIESST). The main objective is to demonstrate that by playing with the nature of the substituent and its position, it is possible to create stronger cohesive forces and receive a more cooperative response from the compounds.

Importantly, recent studies have shown that the electronic influence of a substituent on a coordinated metal ion depends on its position on the ligand framework.[37, 38]

This article complements the literature and helps to understand how the SCO behaviors of a complex is influenced by the nature of its ligands.

2 EXPERIMENTAL SECTION

With this background in mind, an Fe(II) family of [Fe(NCS)2(L)$_2$phen] with L = pyridine or picoline derivative has been synthesized and characterized. Starting from compound [Fe(NCS)$_2$(py)$_2$phen] in Fig. 1, several chemical modifications can be made, either on the phenanthroline or on the pyridine ligands. In this work, we focused on substituted pyridine ligands (Fig. 2).

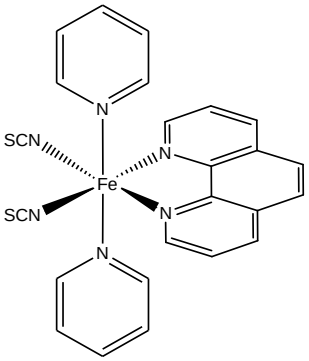

Fig. 1: Schematic representation of the iron(II) molecular unit involved in the [Fe(NCS)$_2$(py)$_2$phen] crystals.

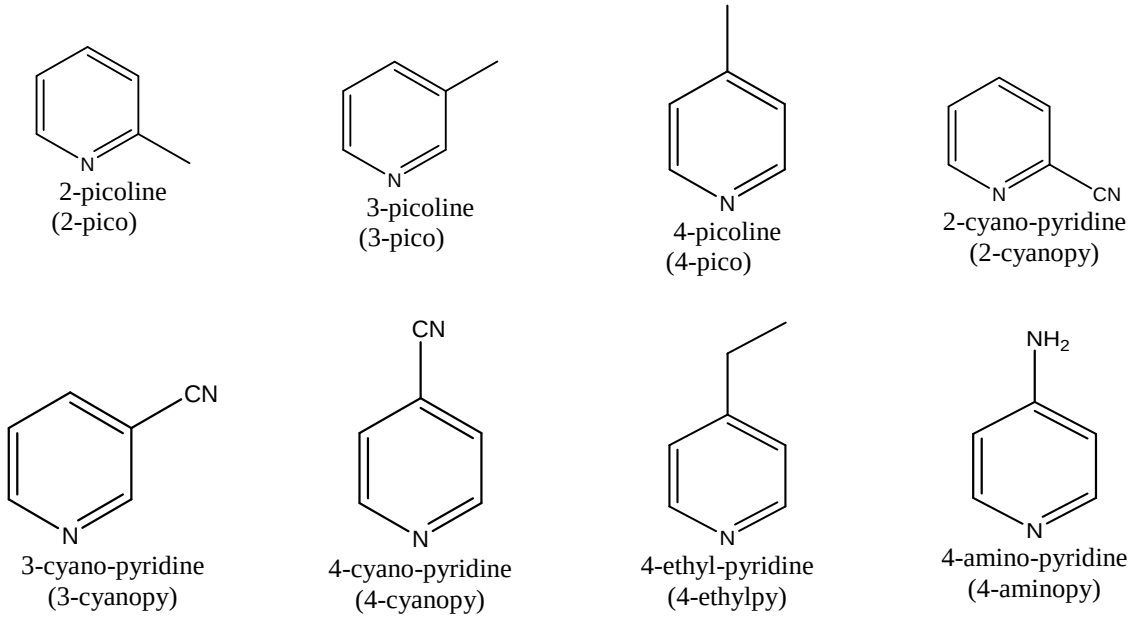

Fig. 2: Schematic representation of de ligands discussed in this work.

Synthesis

General: All syntheses were carried out under nitrogen according to the synthesis scheme below.

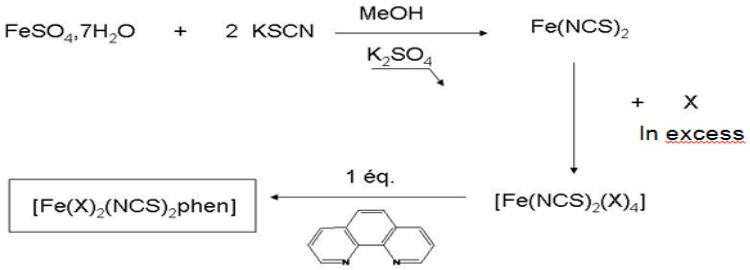

Fig 3: Synthesis scheme.

We succeeded in synthesizing 3 pure complexes by this procedure, [Fe(NCS)$_2$(py)$_2$phen] (1), [Fe(NCS)$_2$(4-pico)$_2$phen] (2) and [Fe(NCS)$_2$(4-ethylpy)$_2$phen] (3). Indeed, for ligands having a substituent in position 2 or 3, a large steric hindrance causes the dissociation of ligand X after the addition of phenanthroline, leaving a vacant coordination site for another phenanthroline molecule.

[Fe(NCS)$_2$(py)$_2$phen] (1): The preparation of the complex has been described earlier by Erickson and Sutin,[41] but slightly modified. The hydrated iron(II) perchlorate being replaced by Iron(II) Sulfate $FeSO_4$, $7H_2O$. The synthesis of the complex [Fe(NCS)$_2$(py)$_2$phen] was done by reacting 0.278 g (1.10^{-3} mol) of $FeSO_4 \cdot 7H_2O$ and 0.194 g (2.10^{-3} mol) of KSCN in dry and freshly distilled methanol (5 ml). The precipitated K_2SO_4 was filtered off. The solution was added to 5 mL of pyridine. The mixture became yellow after incorporation of pyridine. The mixture was stirred during 30 mn and gradually dropped to a solution containing 0.180 g (1.10-3 mol) of 1,10-phenanthroline in 6 mL of pyridine. Purple powder formed from the solution was filtered off and dried under vacuum (See Figure. 3). The elemental analysis of C, H, N, S was performed, and the results agreed well with the calculated data. For [Fe(py)$_2$(NCS)$_2$phen]: Calculated (%) C, 57.25; H, 3.69; N, 16.53; S, 11.80; found : C, 57.61; H, 3.72; N, 16.54; S,11.83.

[Fe(NCS)$_2$(4-pico)$_2$phen] (2): Compound **2** was synthesized according to the same procedure, replacing the pyridine by 4-picoline. The intermediate solution was green/black in colour, and the final precipitated was purple. The elemental analysis of C, H, N, S fit the calculated data. For **2**: Calculated (%): C, 59.54; H, 4.39; N, 15.56; S, 10.96; found: C, 59.18; H, 4.49; N, 15.2; S, 9.50.

[Fe(NCS)$_2$(4-ethylpy)$_2$phen] (3): Compound **3** was synthesized according to the same procedure used for **1**, replacing the pyridine by 4-ethylpyridine. The intermediate solution was orange in colour, and the final precipitated was purple. Here also, the elemental analysis of C, H, N, S fit the calculated data. For **3**: Calculated (%): C, 61.65; H, 5.07; N, 14.63; S, 10.00; found: C, 61.65; H, 5.11; N, 14.50; S, 10.08.

Magnetic and Photomagnetic Studies

Magnetic susceptibility data were collected using a Quantum Design MPMS 5 SQUID magnetometer under an applied field of 1 T. All measurements were performed on homogenous polycrystalline samples and in the temperature range 10 to 290 K. Diamagnetic corrections for the sample holder and the material (using Pascal constants) were applied. Photomagnetic measurements were performed with a set of photo-diodes coupled through an optical fiber to the cavity of a MPMS-55 Quantum Design SQUID magnetometer operating at 2 T. It was noted that there was no change in the data due to heating of the sample. The suspended crystalline sample was prepared in a thin layer (~0.1 mg) to promote full penetration of the irradiated light. The sample mass was obtained by comparison with the thermal spin transition curve measured on a larger accurately weighed polycrystalline sample. The calculated mass is of course approximate, however the adequacy between the bulk and thin layer magnetic measurements is reasonable, taking into account the fact that the data correction of such low amount of sample is challenging. Our previously published standardized method for obtaining LIESST data was followed.[33-35] The sample was first slow cooled to 10 K, ensuring that potential trapping of HS species at low temperatures did not occur. Irradiation was carried out at a set wavelength and the power of the sample surface was adjusted to 5 mW cm^{-2}. Once photo-saturation was reached, irradiation was ceased and the temperature increased at a rate of 0.3 $K.min^{-1}$ to ~100 K and the magnetization measured every 1 K to determine the T(LIESST) value given by the extreme of the $\delta \chi_M T / \delta T$ *versus* T curve for the relaxation. The T(LIESST) value describes the limiting temperature above which the light-induced magnetic high-spin information is erased in a SQUID cavity. In the absence of irradiation, the magnetism was also measured over the temperature range 10 – 290 K to follow the thermal spin transition and to obtain a low temperature baseline. In addition to *T*(LIESST) measurement. Kinetic studies were performed by irradiating the sample at 10 K until photo-saturation, then, under constant irradiation the sample was warmed to a desired temperature around the *T*(LIESST) region. At the desired temperature, irradiation ceased and the decay of the magnetization signal was followed for several hours, or until complete relaxation back to the low-spin baseline.

Optical reflectivity measurements

Variable temperature reflectivity measurements were performed using a home-built instrument coupled with a CVI spectrometer. This equipment can collect the reflectivity spectra in the 450–950 nm range at a given temperature, and also follow the temperature dependence of the signal at a selected wavelength (±2.5 nm) between 5 K and 290 K. The instrument is also equipped with an optical detector, which collected the whole reflected intensity and gave the total reflectivity signal as a function of temperature. The source of white light consisted of a halogen lamp emitting between 300 and 2400 nm. This analysis was performed directly on a thin layer of the solid samples in the form of a polycrystalline powder without any dispersion in a matrix. It was checked that no change in the powder was recorded after a thermal cycle. Spectra were collected at a range of temperatures with the sample under constant irradiation.

X-ray diffraction

A single crystal of dimensions 0.30 × 0.25 × 0.20 mm was mounted on a Bruker-Nonius Kappa CCD area detector system and the diffraction data were collected at

100 K temperature by using graphite-monochromated Mo Kα radiation (λ = 0.71073 Å). The absorption correction made by Empirical method (using intensity measurements) SCALEPACK and the crystal structure solved by the direct method using the program SHELXS-97. The refinement and all further calculations were carried out using SHELXL-97 and SHELXL-2013.[42] Hydrogen atoms bound to the carbon atoms of the aromatic rings were set in calculated positions and refined as riding atoms with a common fixed isotropically thermal parameter. Full-matrix least-squares refinements on F^2, carried out by minimizing the function $\sum w(|F_o| - |F_c|)^2$, reached convergence with values of the discrepancy indices given in Table 1. The graphical manipulations were performed using *Mercury* software.[43]

3 RESULTS AND DISCUSSION

3.1 Structural Characterization

Crystals of the intermediate complex, [Fe(3-cyanopy)$_4$(NCS)$_2$] suitable for X-ray analysis were obtained was obtained by slow evaporation of the methanol solution. Single-crystal X-ray diffraction reveals that this compound crystallizes in the orthorhombic space group *Pc2$_1$n* with four formula units per cell. The crystal data of the compound are summarized in Table 1. Its molecular structure is shown in Fig. 4. It is a discrete neutral monomer, where its asymmetric unit corresponds to the formula unit and contains one Fe(II) cation, two isothiocyanate anions, and four 3-cyanopyridine ligands. Each Fe(II) cation has a slightly distorted FeN6 octahedral coordination environment formed by four (N2, N3, N5, and N6) nitrogen atoms of four 3-cyanopyridine ligands and two (N1 and N4) nitrogen atoms of two isothiocyanates. The two thiocyanate ligands are coordinated through their nitrogen atoms and are quasi-linear [S1-C1-N1 = 178.65(18)° and S2-C2-N4 = 179.60(17)°], while the Fe-NCS bonds are bent [Fe1-N1-C1 = 163.18(15)° and Fe1-N4-C2 = 175.20(13)°].

Fig. 5 and Fig. 6 show the Packing of the molecules in [Fe(3-cyanopy)$_4$(NCS)$_2$], with different intermolecular contacts.

Table 1: Crystal Data and Structure Refinement for title compound [Fe(3-CNpy)$_4$(SCN)$_2$]

Chemical formula	$C_{26}H_{16}FeN_{10}S_2$
M	588.46
Crystal system, space group	Orthorhombic, *Pc2$_1$n*
Temperature (K)	100
a, *b*, *c* (Å)	10.198 (1), 13.033 (1), 20.374 (2)
V (Å^3)	2707.9 (4)
Z	4
Radiation type	Mo *Kα*
μ (mm^{-1})	0.75
Crystal size (mm)	0.30 × 0.25 × 0.20
Data collection	
Diffractometer	Kappa CCD
Absorption correction	Empirical (using intensity measurements) SCALEPACK
T_{min}, T_{max}	0.807, 0.865
No. of measured, independent and observed [$I > 2\sigma(I)$] reflections	8890, 5036, 4931
R_{int}	0.031
$(\sin \theta/\lambda)_{max}$ (Å^{-1})	0.649
Refinement	
$R[F^2 > 2\sigma(F^2)]$, $wR(F^2)$, *S*	0.023, 0.062, 1.12
No. of reflections	5036
No. of parameters	352
No. of restraints	1
H-atom treatment	H-atom parameters constrained
$\Delta\rho_{max}$, $\Delta\rho_{min}$ (e Å^{-3})	0.26, −0.46
Absolute structure	Flack H D (1983), Acta Cryst. A39, 876-881
Absolute structure parameter	0.021 (8)

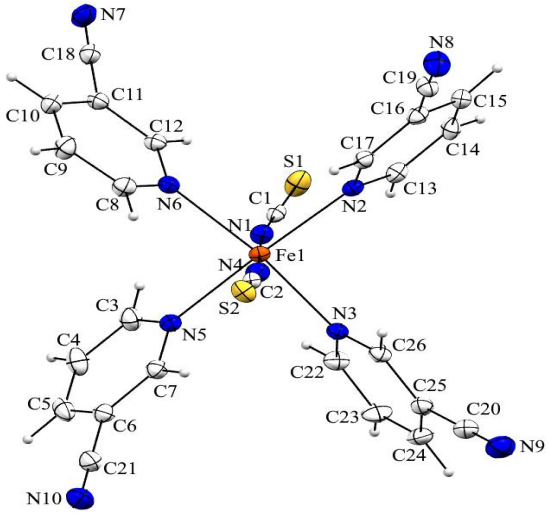

Fig. 4: The molecular structure of the Fe(3-cyanopy)$_4$(NCS)$_2$] compound, showing the atom labeling. Displacement ellipsoids are drawn at the 50% probability level.

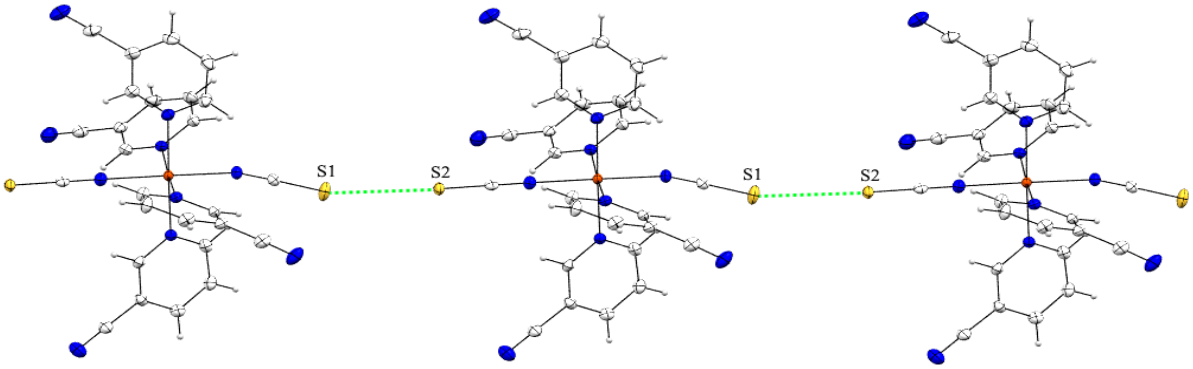

Fig. 5: View of the packing showing the shortest S···S contacts (green broken lines) between the [Fe(3-CNpy)4(SCN)2] monometallic units.

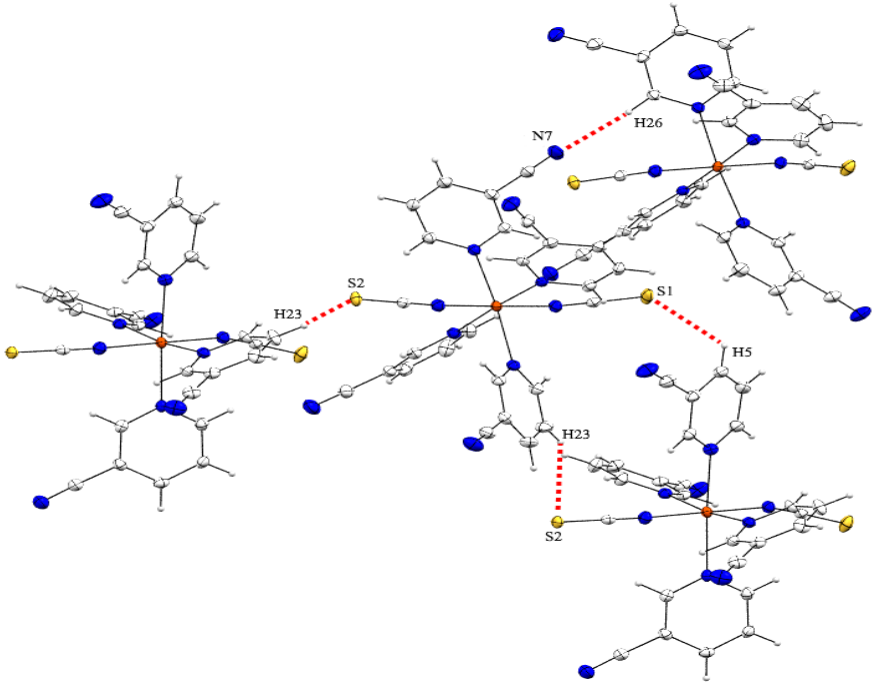

Fig. 6: View of the significant hydrogen bonds (red broken lines) within the crystal structure.

3.2 Magnetic Characterizations

The variable-temperature magnetic susceptibility data for the complexes were obtained between 10 K to room temperature using the using a Quantum Design MPMS 5 SQUID magnetometer under an applied field of 1 T. The thermal dependence of the $\chi_M T$ product (in which χ_M stands for the molar magnetic susceptibility and T the temperature) for the three complexes is shown in Figure 7. For compound **[Fe(NCS)$_2$(py)$_2$phen] (1)**, the $\chi_M T$ product at room temperature is of about 3.5 cm^3Kmol^{-1}, as expected for a fully occupied quintet paramagnetic iron(II) metal ion in the HS state (S = 2, $t_{2g}^4e_g^2$). Upon cooling to about 125 K, the magnetic response drops suddenly and reaches 0.2 cm^3Kmol^{-1} at 75 K, which suggests that essentially all iron(II) metal sites are LS. This indicates that **1** exhibits an abrupt spin transition taking place at $T_{1/2}$ = 105 K. Upon warming, the same step process is followed without any hysteresis regime. For **[Fe(NCS)$_2$(4-pico)$_2$phen] (2)**, upon cooling, the $\chi_M T$ values remain approximately constant down to 150 K (3.05 $cm^3mol^{-1}K$), at which point the magnetic signal gradually decreases to reach 0.2 cm^3Kmol^{-1} in the temperature range 150 – 75 K. In the warming mode, the $\chi_M T$ product of **2** smoothly increases and the magnetic data perfectly correspond to those obtained in the cooling mode, showing that a complete gradual spin transition occurs at $T_{1/2}$ = 112 K without thermal hysteresis. For **[Fe(NCS)$_2$(4-ethylpy)$_2$phen] (3)**, upon cooling from room temperature to 30 K, the $\chi_M T$ value of 3.5 is invariant to temperature, indicative of the HS Fe(II) forms. The rapid decrease of $\chi_M T$ product below 30 K is due to the zero-field splitting of the HS iron(II) ion.[44, 45] The magnetic behavior of the three compounds (Fig.7) suggests that the ligand field strength is modulated by substitution inside the ligand molecule. This indicates that alkyl substitution on the pyridine ligand has good potential to improve SCO properties within Fe(II)-SCO systems. This will be discussed later.

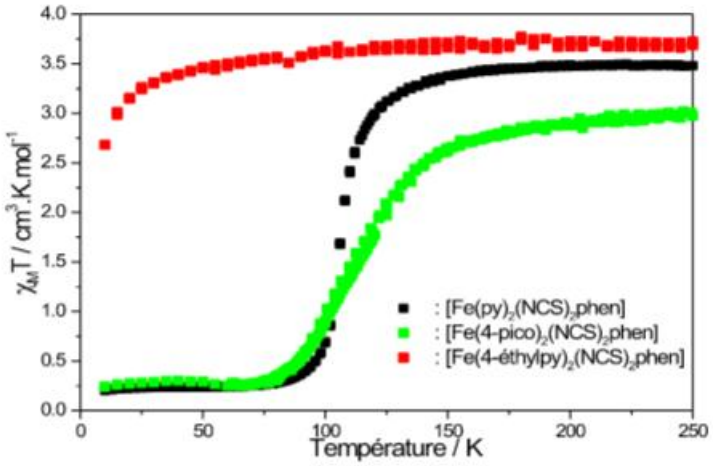

Fig. 7: Magnetic properties as function of the temperature for 1-3.

3.3 Optical Diffused Reflectivity and Photomagnetic investigations

Thermal spin-crossover can be monitored by following the visible spectrum of the powder sample. Changes in the diffuse absorption spectra measured as a function of temperature and light irradiation were used to follow the relative amounts of HS and LS iron(II) species. Typical spectra, recorded for **1** is presented in Fig. 8. The first part of the figure shows the evolution of the spectra between 250 and 70 K. It can be observed that, when decreasing the temperature, a broad band present at 750–850 nm tends to disappear, whereas a new band, sharper, appears at 700 nm. The absorptions in the 600,700 nm region can be assigned to both MLCT and d–d transitions of the LS material, namely the $^1A_1 \rightarrow {}^1T_1$. On the other hand, the broad peak at 800 nm is attributed to a d-d band of the HS state of the compound, namely the $^5T_2 \rightarrow {}^5E$.

At temperatures below 80 K, the reverse process occurs with a new increase in the 800 nm band associated to a decrease of the band at 650 nm. This experiment suggests that at the surface of the sample some light-induced effect occurs at low temperature along with the LIESST process. In fact, when the temperature is sufficiently low, the intensity of the light source used to record the reflectivity signal is large enough to photoswitch the LS state into a HS state as a result of the very slow relaxation time. Compound **1** and **2** exhibit the same general behavior.

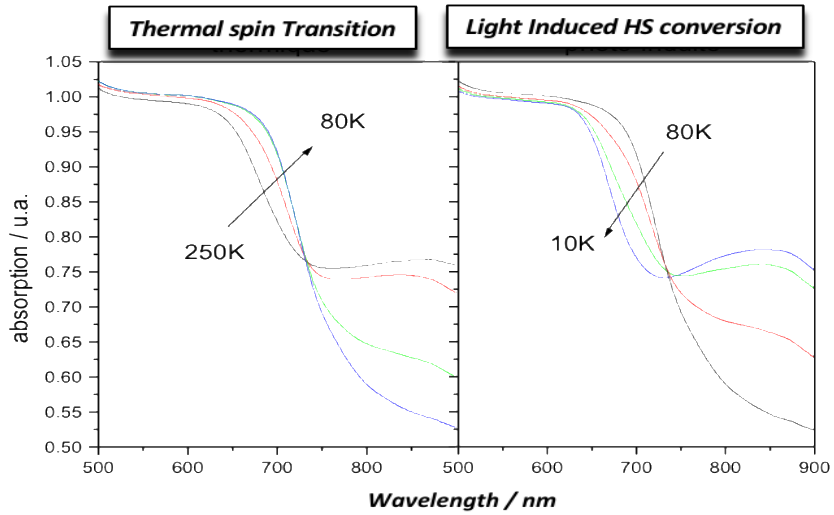

Fig. 8: Thermal evolution of the diffuse absorption spectra of compound 1 and 2 along the thermal SCO phenomenon from 250 – 80 K (left) and the light-induced photoconversion process from 80 – 10 K (right).

Besides the most commonly used thermally induced SCO, it is also possible to control the HS and LS populations of SCO metal complexes with selective light into appropriate ligand-field (d–d) or charge-transfer absorption bands with visible or near-infrared light. This phenomenon is commonly known as light induced excited spin state trapping (LIESST) for the LS → HS conversion[46] or reverse-LIESST for the HS → LS conversion.[47] Experimentally, the photoinduced SCO was investigated by using SQUID magnetometer coupled to a CW optical source. The method used here, is to detrappe the metastable HS by thermal excitation, after photo irradiation at 10 K: on warming, the system jumps over the energy barrier and relaxes to the stable LS state al. This have led to the determination of a limiting temperature value, coined **T**(LIESST) for all the compounds under investigation.

The effect of light irradiation on compounds **1** and **2** was studied. For all of them, irradiations at 405, 510, 650, 830 and 980 nm were tested and a 650 nm irradiation induced the most efficient photoconversion, leading to an increase of the magnetic signal at 10 K (Figure 9). Using the *T*(LIESST) procedure, after irradiation until the photo-saturation at 10 K, the light was switched OFF and the temperature was increased with a standard value of the temperature scan rate, 0.3 K/min (0.005 K/s), to allow the comparison of the photomagnetic properties of compounds. The $\chi_M T$ product first increases upon warming from 10-30 K due to zero-field splitting of the high spin iron(II) ion.[44, 45] Then after a plateau, $\chi_M T$ value decreases sharply. T(LIESST) is determined by the minimum of the derivative $\partial(\chi_M T)/\partial T$ versus T (Inset, Figure 9). Values of **T**(LIESST) for **1** and **2** are found to be almost the same for the two compounds: T(LIESST) has been recorded at 54 K . It should, however, be noticed that the amount of iron in the photoexcited high-spin state is not the same for **1** and **2**, only compound **1** exhibits a quantitative photoexcitation.

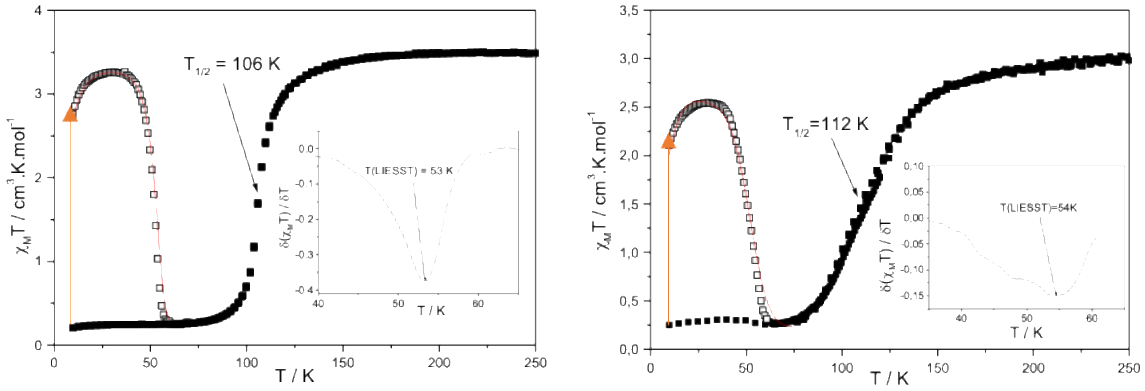

Figure. 9: Temperature dependence of the $\chi_M T$ product of 1 and 2: data recorded (□) without irradiation, (↑) under irradiation at 10 K and (☐) T(LIESST) measurement in the warming mode when the laser switched OFF. The Inset displays the derivative $\partial(\chi_M T)/\partial T$ versus T.

4 CONCLUSIONS

In this work we have reported the thermal and light-induced magnetic properties of a family of alkyl-substituted pyridine ligand iron(II) complexes, $[Fe(NCS)_2(L)_2phen]$ with L = pyridine (**1**), 4-picoline (**2**) or 4-ethylpyridine (**3**). For all of them, we have systematically investigated the thermal spin-crossover (SCO) properties and the stability of the photo-induced HS state through the determination of the T(LIESST) value associated with the Light-Induced Excited Spin-State Trapping (LIESST) effect. The compound **1** displays a complete and abrupt spin transition. For the complex **2**, the thermal SCO properties show a gradual character. For compound **3**, the HS ($^5T_2$) remains the stable ground state at all the temperature range. No SCO is observed because the ligand field strength is too weak to meet the critical SCO condition. This series of data confirms the role of ligand design affecting the thermal and light-induced spin transition in mononuclear iron(II) complexes. We have demonstrated that the ligand field strength is modulated by substitution inside the ligand molecule. It is obvious that the alkyl substituent exerts a strong steric effect in the complex. However, the alkyl substituents have been introduced in position 4 of the aromatic pyridine ring in order to minimize the distortion of the metal ion environment and focus study only on the effects of the inductive character of the substituent. Exchange of H for CH_3 and C_2H_5 in the 4-position of the pyridine ligand weakens the ligand field strength due to steric hindrance. Indeed, when we replace H by an ethyl group in the 4-position of the pyridine ligand, the strength of the average ligand field acting at the central iron atom is weakened such that the condition for thermal SCO to occur is now fulfilled. This is corroborated by the studies conducted by Gütlich and coworkers on $[Fe(Y\text{-}phen)_3]X_2$ complexes.[11],[48],[49] It has been illustrated with this group of complexes that exchange of H for CH_3 in either the 2- or 9-position of the three phen ligands weakens the ligand field strength due to steric hindrance (whereby the metal–donor-atom distance is elongated) and the LS behavior of $[Fe(phen)_3]X_2$ turns to SCO behavior of the tris(2-CH3-phen) complex. In addition, if both the 2- and 9-positions of the three phen ligands are substituted by CH_3 the steric hindrance is even stronger and weakens the ligand field strength further, yielding HS behavior of the tris[2,9-(CH3)2] complex down to very low temperatures.[11],[48],[49] Finally, let us mention that the effects of the alkyl substituents in the pyridine ligand sphere extend from a more or less distinct $T_{1/2}$ shift towards higher or lower temperatures with a change in the transition slope for **1** and **2** and complete suppression of the spin transition for **3** exhibiting only the HS state at all temperatures. The cooperative thermal SCO regime is also strongly affected by the ligand substituent. It was found that a combination of steric hindrance due to bulkiness and an electronic influence of the substituent on the basicity of the coordinating N-atom is responsible for the influence on the SCO behavior.[11][36-40],[48, 49]

Our photomagnetic studies show that T(LIESST) is not affected by the ligand substuent while $T_{1/2}$ is shift to higher or lower temperatures depending of the substituent. T(LIESST) value is almost the same for **1** and **2** (≈ 54 K) while $T_{1/2}$ varies from 106 K for **1** to 112 K for **2**. This is in line with previous conclusions suggesting that the photomagnetic properties are governed at the molecular scale while the thermal spin crossover regime is driven by both the ligand field and crystal packing effects.

Substitution in the 2-position of the pyridine or phenanthroline ligand induces high steric strain that prevent any coordination to the metal site.

Similar studies on the effects of chemical influences on the SCO behavior using a various substituent and their respective positions within the pyridine ligand are currently in progress, where we expect to learn more about the role of ligand design in affecting SCO. In addition, the study of sterically constrained complexes would give insight into the influence of the coordination-sphere distortion on the stability of the light-induced HS state. These investigations are currently under way.

ACKNOWLEDGMENT

We thank the Department of Cooperation and Cultural Action Embassy of France to Dakar-Sénégal, the University of Ziguinchor and its Department of Cooperation and Research, the Ministry of Higher Education and Research of Sénégal (Program FIRST and CNDST) and CAMPUS France. This work was also supported by the University of Bordeaux, the Centre National de la Recherche Scientifique (CNRS), the Region Nouvelle Aquitaine and by the LabEx AMADEus (ANR-10-LABX-42) within IdEx Bordeaux (ANR-10-IDEX-03-02), i.e. the Investissements d'Avenir programme of the French government managed by the Agence Nationale de la Recherche. The ANR is also warmly acknowledge (ANR femtomat n° 13-BS04-002).

REFERENCES

1. Petty MC, Bryce MR, Bloor D. Introduction to Molecular Electronics, Oxford University Press, New York, 1995.
2. Lehn JM. Toward Self-Organization and Complex Matter. Science, 2002; 295(5564): 2400-2403.
3. Ruben M, Ziener U, Lehn JM, Ksenofontov V, Gutlich P, Vaughan GBM. Hierarchical Self-Assembly of Supramolecular Spintronic Modules into 1D- and 2D-Architectures with Emergence of Magnetic Properties. Chemistry A European Journal, 2005; 11(1): 94-100.
4. Fujita M, Oguro D, Miyazawa M, Oka H, Yamaguchi K, Ogura K. Self-assembly of ten molecules into nanometre-sized organic host frameworks. Nature, 1995; 378: 469–47.
5. Yaghi OM, O'Keeffe M, Ockwig NW, Chae HK, Eddaoudi M, Kim J. Reticular synthesis and the

design of new materials. Nature, 2003; 423: 705–714.
6. Breuning E, Ruben M, Lehn JM, Renz F, Garcia Y, Ksenofontov V, Gütlich P, Wegelius E, Rissanen K. Spin Crossover in a Supramolecular Fe4II [2×2] Grid Triggered by Temperature, Pressure, and Light. Angewandte International Edition Chemie, 2000; 39(14): 2504-2507.
7. Spin Crossover in Transition Metal Compounds I−III. In: Topics in Current Chemistry, P. Gütlich, H. A. Goodwin, (Eds.), Springer-Verlag: Berlin, Germany, 2004; 233−235.
8. Halcrow MA. Spin-crossover Materials: Properties and Applications, Ed. John Wiley & Sons, Chichester, UK: 2013.
9. Bousseksou A, Molnar G, Salmon L, Nicolazzi W. Molecular spin crossover phenomenon: recent achievements and prospects. Chemical Society Reviews, 2011; 40(6): 3313-3335.
10. Kahn O, Martinez CJ. Spin-Transition Polymers: From Molecular Materials Toward Memory Devices. Science, 1998; 279(5347): 44-48.
11. Gütlich P, Gaspar AB and Garcia Y. Spin state switching in iron coordination compounds. Beilstein Journal of Organic Chemistry, 2013; 9: 342-391.
12. Kumar KS, Ruben M. Emerging trends in spin crossover (SCO) based functional materials and devices. Coordination Chemistry Reviews, 2017; 346: 176-205.
13. Khusniyarov MM. How to Switch Spin-Crossover Metal Complexes at Constant Room Temperature. Chemistry A European Journal, 2016; 22(44): 15178-15191.
14. Cambi L, Szegö L. Über die magnetische Susceptibilität der komplexen Verbindungen. Berichte der deutschen chemischen Gesellschaft (A and B Series), 1931; 64(10): 2591-2598.
15. Guionneau P. Crystallography and spin-crossover. A view of breathing materials. Dalton Transactions, 2014; 43(2): 382-393.
16. Nicolazzi W, Bousseksou A. Thermodynamical aspects of the spin crossover phenomenon. Comptes Rendus Chimie, 2018; 21: 1060-1074.
17. Collet E, Guionneau P. Structural analysis of spin-crossover materials: From molecules to materials. Comptes Rendus Chimie, 2018; 21: 1133-1151.
18. Boillot ML, Weber B. Mononuclear ferrous and ferric complexes. Comptes Rendus Chimie, 2018; 21 : 1196-1208.
19. Costa JS. Macroscopic methods: Magnetic, optical, and calorimetric techniques. Comptes Rendus Chimie, 2018; 21: 1121-1132.
20. Mascaros JRG, Aromi G, Darawsheh M. Polynuclear Fe(II) complexes: Di/trinuclear molecules and coordination networks. Comptes Rendus Chimie, 2018; 21: 1209-1229.
21. Munoz MC, Real JA. Thermo, piezo, photo and chemo-switchable spin crossover iron(II)-metallocyanate based coordination polymers. Coordination Chemistry Reviews, 2011; 255(17): 2068-2093.
22. Gass IA, Batten SR, Forsyth CM, Moubaraki M, Schneider CJ, Murray KS. Supramolecular aspects of iron(II) crown-dipyridyl spin-crossover compounds. Coordination Chemistry Reviews, 2011; 255(17): 2058-2067.
23. Létard JF. Photomagnetism of iron(ii) spin crossover complexes—the T(LIESST) approach. Journal of Materials Chemistry, 2006; 16(26): 2550-2559.
24. Gütlich P, Goodwin HA. Spin Crossover—An Overall Perspective. Topics in Current Chemistry, 2004; 233: 1-47.
25. Hauser A. Intersystem crossing in Fe(II) coordination compounds. Coordination Chemistry Reviews, 1991; 111: 275-290.
26. Rotaru A, Gural'skiy IA, Molnar G, Salmon L, Demont P, Bousseksou A. Spin state dependence of electrical conductivity of spin crossover materials. Chemical Communications, 2012; 48(35): 4163-4165.
27. Shepherd HJ, Quintero CM, Molnar G, Salmon L, Bousseksou A, In: M. A. Halcrow (Eds.), Spin-Crossover Materials, Properties and Applications, John Wiley & Sons, Ltd, 2013; 347–373.
28. Lacroix PG, Malfant I, Real JA, Rodriguez V. From Magnetic to Nonlinear Optical Switches in Spin-Crossover Complexes. European Journal of Inorganic Chemistry, 2103; 2013(5-6): 615-627.
29. Manrique-Juarez MD, Rat S, Salmon L, Molnar G, Quintero GCM, Nicu L, Shepherd HJ, Bousseksou A. Switchable molecule-based materials for micro- and nanoscale actuating applications: Achievements and prospects. Coordination Chemistry Reviews, 2016; 308: 395-408.
30. Ksenofontov V, Levchenko G, Spiering H, Gütlich P, Létard JF, Bouhedja Y, Kahn O. Spin crossover behavior under pressure of Fe(PM-L)2(NCS)2 compounds with substituted 2′-pyridylmethylene 4-anilino ligands. Chemical Physics Letters, 1998; 294(6): 545-553.
31. McGravey JJ, Lawthers I. Photochemically-induced perturbation of the 1A ⇌5T equilibrium in Fe11 complexes by pulsed laser irradiation in the metal-to-ligand charge-transfer absorption band. Journal of the Chemical Society, Chemical Communications, 1982; 16: 906-907.
32. Decurtins S, Gütlich P, Köhler CP, Spiering H, Hauser A. Light-induced excited spin state trapping in a transition-metal complex: The hexa-1-propyltetrazole-iron (II) tetrafluoroborate spin-crossover system. Chemical Physics Letters, 1984; 105(1): 1-4.
33. Bonhommeau S, Molnár G, Goiran M, Boukheddaden K, Bousseksou A. Unified dynamical description of pulsed magnetic field and pressure effects on the spin crossover phenomenon. Physical Review B, 2006; 74(6): 064424.
34. Lefter C, Tan R, Dugay J, Tricard S, Molnar G, Salmon L, Carrey J, Nicolazzi W, Rotaru A,

Bousseksou A. Unidirectional electric field-induced spin-state switching in spin crossover based microelectronic devices. Chemical Physics Letters, 2016; 644: 138-141.
35. Halder GJ, Kepert CJ, Moubaraki B, Murray KS, Cashion JD. Guest-Dependent Spin Crossover in a Nanoporous Molecular Framework Material. Science, 2002; 298(5599): 1762-1765.
36. Phonsri W, Macedo DS, Vignesh KR, Rajaraman G, Davies CG, Jameson GNL, Moubaraki B, Ward JS, Kruger PE, Chastanet G, Murray KS. Halogen Substitution Effects on N2O Schiff Base Ligands in Unprecedented Abrupt FeII Spin Crossover Complexes. Chemistry A European Journal, 2017; 23(29): 7052-7065.
37. Halcrow M. The Effect of Ligand Design on Metal Ion Spin State—Lessons from Spin Crossover Complexes. Crystals, 2016; 6(58): 1-20.
38. Feltham HLC, Barltrop AS, Brooker S. Spin crossover in iron(II) complexes of 3,4,5-tri-substituted-1,2,4-triazole (Rdpt), 3,5-di-substituted-1,2,4-triazolate (dpt), and related ligands. Coordination Chemistry Reviews, 2017; 344: 26-53.
39. Nassirinia N, Amani S, Teat SJ, Roubeau O, Gamez P. Enhancement of spin-crossover cooperativity mediated by lone pair–π interactions and halogen bonding. Chemical Communications, 2014; 50(8): 1003-1005.
40. Baldé C, Paradis N, Desplanches C, Chastanet G. Switchable Heteroleptic Mononuclear Iron(II) Complexes as Versatile Molecular Building Block. European Journal of Inorganic Chemistry, 2018; 2018(19): 2004-2010.
41. Erickson NE, Sutin N. The So-Called cis-trans Isomerism of Bis(isothiocyanato) tetra(pyridine) iron(II). Inorganic Chemistry, 1966; 5(10): 1834-1835.
42. Sheldrick GM. A short history of SHELX. Acta Crystallographica Section A, 2008; A64: 112‑122.
43. Macrae CF, Bruno IJ, Chisholm JA, Edgington PR, McCabe P, Pidcock E, Rodriguez-Monge L, Taylor R, van de Streek J and Wood PA. New Features for the Visualization and Investigation of Crystal Structures. Journal of Applied Crystallography, 2008; 41: 466-470.
44. Boca R. Zero-field splitting in metal complexes. Coordination Chemistry Reviews, 2004; 248(9–10): 757-815.
45. Létard JF, Carbonera C, Courcot E, Costa JS. A typical example of a photomagnetic study carried out on a spin-crossover material. Bulletin of Materials Science, 2006; 29(6): 567–571.
46. Decurtins S, Gütlich P, Kohler CP, Spiering H, Hauser A. Light-induced excited spin state trapping in a transition-metal complex: The hexa-1-propyltetrazole-iron (II) tetrafluoroborate spin-crossover system. Chemical Physics Letters, 1984; 105(1): 1-4.
47. Hauser A. Reversibility of light-induced excited spin state trapping in the Fe(ptz)6(BF4)2, and the Zn1−xFex(ptz)6(BF4)2 spin-crossover systems. Chemical Physics Letters, 1986; 124(6): 543-548.
48. Fleisch J, Gütlich P, Hasselbach KM, Müller W. High Spin-Low Spin Transition In Substituted Phenanthroline Complexes of Iron (II). Journal de Physique Colloques, 1974; 35(6): 659-662.
49. Gütlich P, Hauser A, Spiering H. Thermal and Optical Switching of Iron(II) Complexes. Angewandte International Edition Chemie, 1994; 33(20): 2024-2054.